The orientation and charge of water at the hydrophobic oil droplet-water interface

Robert Vacha,[†] Steven W. Rick,[‡] Pavel Jungwirth,[¶] Alex G. F. de Beer,[§] Hilton B. de Aguiar,[§] Jean-Sebastien Samson,[§] and Sylvie Roke[*,‖,§]

Department of Chemistry, Lensfield Road, Cambridge, CB2 1EW, United Kingdom, Department of Chemistry, University of New Orleans, New Orleans, LA, 70148, USA, Institute of Organic Chemistry and Biochemistry, Academy of Sciences of the Czech Republic and Center for Complex Molecular Systems and Biomolecules, Flemingovo nam. 2, 16610 Prague, Czech Republic, Max-Planck-Institut fuer Metallforschung, Heisenbergstrasse 3, 70569 Stuttgart, Germany., and Institute of Bioengineering, School of Engineering, École Polytechnique Fédérale de Lausanne (EPFL), 1015 Lausanne, Switzerland.

E-mail: sylvie.roke@epfl.ch

[*]To whom correspondence should be addressed

[†]Department of Chemistry, Lensfield Road, Cambridge, CB2 1EW, United Kingdom

[‡]Department of Chemistry, University of New Orleans, New Orleans, LA, 70148, USA

[¶]Institute of Organic Chemistry and Biochemistry, Academy of Sciences of the Czech Republic and Center for Complex Molecular Systems and Biomolecules, Flemingovo nam. 2, 16610 Prague, Czech Republic

[§]Max-Planck-Institut fuer Metallforschung, Heisenbergstrasse 3, 70569 Stuttgart, Germany.

[‖]Institute of Bioengineering, School of Engineering, École Polytechnique Fédérale de Lausanne (EPFL), 1015 Lausanne, Switzerland.

May 11, 2011

Abstract

We established the charge and structure of the oil/water interface by combining ζ-potential measurements, sum frequency scattering (SFS) and molecular dynamics simulations. The SFS experiments show that the orientation of water molecules can be followed on the oil droplet/water interface. The average water orientation on a neat oil droplet/water interface is the same as the water orientation on a negatively charged interface. pH dependent experiments show, however, that there is no sign of selective adsorption of hydroxide ions. Molecular dynamics simulations, both with and without intermolecular charge transfer, show that the balance of accepting and donating hydrogen bonds is broken in the interfacial layer, leading to surface charging. This can account for the negative surface charge that is found in experiments.

Introduction

It is common wisdom that water and oil do not mix and can at best form a metastable emulsion. These metastable emulsions can, however, persists for days, months, or even years. What makes these emulsions long-lived, is not clear. Surface charges most likely play a role,[1,2] but as long as we do not fully understand the molecular structure of the interfaces between water and hydrophobic media, such as air, oil, or non-polar regions of protein surfaces, the reason for emulsion stability cannot be clarified. In order to understand the surprisingly longevity of oil droplets in pure water it is crucial to establish the orientation of water molecules and the charge distribution at the oil/water interface.

Spectroscopic experiments, surface tension measurements, and molecular simulations done on planar air/water interfaces suggest that the water surface is weakly attractive for protons, and less so for the OH^- ion[1].[3–15] On the other hand, a variety of other experiments on e.g. air bubbles, oil

[1]It should be mentioned in this context, that simulations of water next to rigid hydrophobic interfaces showed a stronger interfacial propensity of OH^- than for the water-vapor interface.[3,4] Later simulations, however, demonstrated that this is primarily due to the rigidity of the hydrophobic wall, since the strong interfacial adsorption of hydroxide disappears for soft oil/water interfaces.[5]

droplets in water, and water droplets in air or oil, however, report a negative surface charge[16–28] (and references therein). The latter negative surface charge can be derived from (dynamic) electrophoretic mobility measurements and can be expressed either as charge or ζ-potential.[29,30] The negative charge or ζ-potential is pH dependent. It is commonly observed that the ζ-potential increases to more negative values when the pH is increased.[17,27,31,32] This pH dependence of the ζ-potential has been interpreted in terms of a very strong surface adsorption of hydroxide ions and the Gibbs free energy of adsorption for OH^- has been estimated -62 kJ/mol.[17]

Depending on which method is used, OH^- is either found to have a very high surface affinity or a very low surface affinity. Part of the discrepancy might be due to subtle differences between the various approaches used to investigate aqueous interfaces. Experiments on emulsions are favorable since droplet oil/water interfaces are created in a liquid environment (without exposure to air), and the typical surface area can be enormous (1 ml of 1 vol% of oil droplets with a radius of 100 nm contains 3000 cm^2 of surface area). The disadvantage of studies on emulsions is that the observable is usually a macroscopic quantity that is not necessarily restricted to the few monolayers that make up the surface of the droplet (such as pH, ζ-potential, or projected surface charge).[17,22,32,33] The ζ-potential is the potential that results from charge present within the hydrodynamically stagnant fluid layer that surrounds a particle or droplet (illustrated in Fig 1). The position of this layer is called the slip plane and the exact position within the liquid is unidentified. Depending on the nature of the interface it is usually estimated to be between 0.3 - 6 nm from the Gibbs Dividing Surface (GDS).[29] On the other hand, experiments on planar aqueous interfaces with surface specific second harmonic (SH) and sum frequency (SF) generation can probe the interfacial structure typically up to a depth of $\sim$1 nm.[7,10,34–38] SHG experiments have found that the air/water interface is weakly attractive to protons,[7,10] while it was concluded from SFG experiments on the hydrophobic solid/water interface that hydroxide ions adsorb preferentially at the surface with a Gibbs free energy of adsorption of -45 kJ/mol.[38] The surface areas probed in these methods are determined by the overlap area of the laser pulses. For pulses with a diameter of 300 μm the probed area will be around 7×10^{-2} mm^2. A concentration of impurities or film

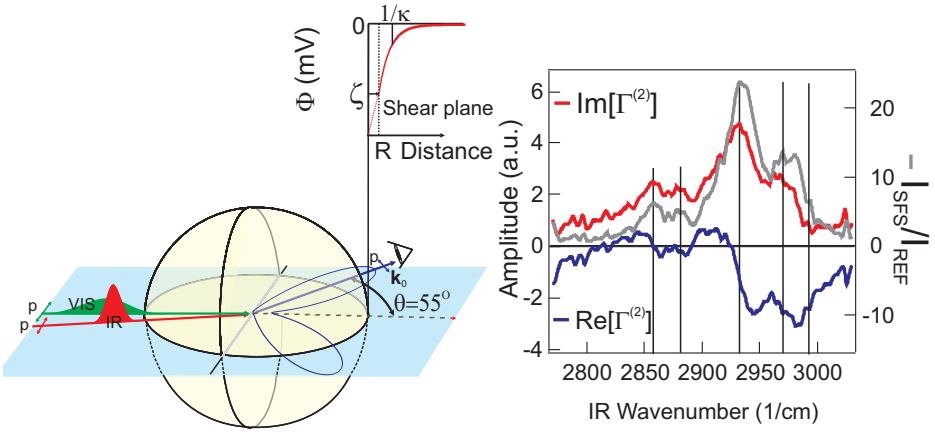

Figure 1: Left: Illustration of sum frequency scattering: a visible and an infrared pulse interact with the oil/water interface around a droplet. At the surface sum frequency photons are created in a broad angular pattern by a simultaneous IR and Raman transition that occurs within the surface molecules. A schematic representation of the surface potential and slip plane is also displayed. Right: The vibrational SF spectrum (grey line, right axis, recorded in *ppp*-polarization combination) of the oil droplet/water interface. The spectrum consists of the vibrational modes of the hexadecane oil molecules with resonances at: 2856 cm^{-1} (sym. CH_2 stretch mode), 2875 cm^{-1} (sym. CH_3 stretch mode), 2930 cm^{-1} (a FR resonance), and 2960 cm^{-1} - 2985 cm^{-1} (asym. CH_3 stretch mode), which are indicated by the vertical lines. The blue and red traces represent the real and imaginary part of the SF response. The droplets are in a 1 vol% emulsion and have an average radius of 337 nm.

defects in the order of one defect/nm^2 can significantly influence the result.[39] It is therefore extremely difficult to unambiguously detect the low concentrations of auto-ionized species H^+ and OH^- of water, at pH=7. Further, it is very challenging to measure the liquid/liquid oil/water interface in a second harmonic or a sum frequency generation reflection mode experiment, due to (i) the difficulty of producing a clean and neat oil/water interface, and (ii) the fact that one of the liquid phases is often absorbing one of the incoming beams. As a consequence, studies that report the structure of water and the pH dependence thereof, have been performed at the air/water interface,[7,10,40–45] on chemically modified hydrophobic solid supports,[36,38] or at water interfaces with a thin layer of (mostly) infrared transparent oil.[35,37,46] Interestingly, although Refs.[36,38] both report pH dependent changes in SFG spectra recorded from the quartz/$CH_3(CH_2)_{17}SiCl_3$/water interface, the measured spectra are different. Furthermore, in Ref.[36] the spectral changes are attributed to originate from an interplay of water molecules present between the quartz and OTS layer and water molecules at the OTS/water interface. In Ref.[38] the observed spectral changes are interpreted as coming from effects induced by the absorption of hydroxide ions. The SF amplitude at 3200 cm^{-1} of the imaginary spectrum was used as a marker of electric field strength, which was correlated to a negative surface potential.

Molecular dynamics (MD) simulations can assist in the interpretation of experiments by providing a picture of aqueous interfaces with atomic spatial and temporal resolution. However, they are limited in system size (having unit cells of several nanometers) and timescales, which typically do not extend beyond a microsecond. Also, the result of a simulation can only be as good as the underlying potential model. Attempts have been made recently to simulate electrophoretic mobilities of oil droplets in water using non-polarizable and polarizable potentials.[47,48] For electrophoresis to occur however, it is essential that there is a finite charge within the slip plane. A static electric field does not induce a steady state flow of charge irrespective of the surface geometry.[28] The potentials used in the above MD simulations do not allow for charge transfer between neighboring water molecules on either side of the slip plane. Therefore, the data on mobility of neutral oil molecules in pure water in a constant electric field using these potentials[47,48] are likely to be incomplete.

The present study starts with surface and molecular sensitive vibrational sum frequency scattering (SFS) on oil droplets dispersed in water. With this approach we can directly measure a large interfacial area and make a direct comparison to the emulsion experiments reported in the literature. Vibrational SFS can be used to retrieve the interfacial vibrational spectrum of the oil droplet/water interface in a surfactant-free emulsion. Since neat oil/water emulsions are made entirely in the liquid phase, a 1 ml emulsion with 100 nm droplets will harbor 3000 cm^2 of clean oil/water interface. The results are therefore not anymore strongly influenced by small amounts of impurities or substrate induced effects. Also, the scattering geometry allows us to measure the signal from a thin slab of D_2O so that IR absorbance is not a major issue.[49] The relative water orientation can be obtained from spectral analysis. A reversal of surface charge results in a change of the water orientation.[50] The net water orientation on an oil/water interface in a pH neutral surfactant free emulsion will be inferred to be similar to the water orientation on an oil droplet/water interface that has been stabilized with negatively charged surfactant. However, pH dependent experiments show that the average interfacial water surface structure remains the same for emulsions prepared at neutral bulk pH up to a bulk pH of 12.5. The increased amount of OH^- is therefore not detectably changing the interface. Using MD simulations with a potential that allows for charge transfer between water molecules, we show that the charge transfer process leads to an effective negative charge at the interface between pure water (without any ions) and oil. Analysis of classical MD simulations of the oil/water interface with a standard force field shows that this charge transfer is due to varying numbers of water molecules with dangling oxygens and dangling hydrogens within the subsequent water layers that form the oil/water interface.

Experimental procedures

The SF scattering experiments were performed using IR pulses centered around $\sim$2900 cm^{-1} (8 - 12 μJ, 150 fs, FWHM bandwidth 120 cm^{-1}) spatially and temporally overlapped with 800 nm VIS pulses (8 - 15 μJ, FWHM bandwidth 5 - 13 cm^{-1}) in a cuvette containing the emulsion. See Ref.[51] for more information on the laser systems, and Ref.[52] for more information on the optical

layout of the SF scattering setup. The oil-in-water emulsions were made by mixing a 1 vol% of oil with 99 vol% pH neutral D_2O (Fig 1), D_2O with surfactant (Fig. 2), or D_2O with dissolved NaOD with a certain pH in a two step process at 293 K. In this process 4 mL of solution was first mixed in a 4 mL vial using a hand-held homogenizer (TH, OMNI International) for 5 mins, after which they were placed for 15 min. in an ultrasonic bath (35 kHz, 400 W, Bandelin). The emulsions with fixed droplet size and different bulk pH of Fig 1 and Fig 3 were prepared by diluting a stock emulsion of 2 vol% oil in D_2O at pH 7 with D_2O at a certain pH. The resultant droplets had a mean radius of 337 nm, and a polydispersity index (PDI) of < 0.17. Droplet size and ζ-potential were determined using a Malvern ZS nanosizer. n-hexadecane ($\geq$99%, Merck), d_{34}-hexadecane (98% D, Cambridge Isotope), D_2O (99 % D, Aldrich), d_{25}-SDS (98% D, Cambridge Isotope), CTAB ($\geq$99%, Acros), d_{33}-CTAB (99% D, CDN Isotopes) and NaOD (99.5%, Aldrich) were used as received. Sodium dodecylsulfate (SDS) ($>$ 99%, Alfa Aesar) was purified by multiple recrystallization cycles in water and ethanol until the surface tension on water at a total concentration of 4 mM SDS (measured with a Wilhelmy plate method) was no longer changing (see Ref.[53]). Glassware was cleaned with a 3:7 H_2O_2:H_2SO_4 solution, after which it was thoroughly rinsed with ultra pure water (0.053μS/cm, TKA) to remove residual chemicals.

Simulation methods

All molecular dynamics simulations were performed using the GROMACS program package version 4.0.5.[54] Each system contained 6000 water molecules placed in a prismatic cell of dimensions 4.0 x 4.0 x 25.0 nm. After 10 ns equilibration time the free space was filled with 486 decane molecules. The whole system was heated up to 400 K and after 10 ns of equilibration it was cooled back to 300 K. After 20 ns of additional equilibration, 100 ns production runs were carried out with 2 fs time steps. In different runs we obtained after equilibration two distinct types of the water/decane interface. The first one had decane molecules oriented perpendicular to the interface, while the second one had decane oriented parallel to the interface. We simulated both types, which did not inter convert within the 100 ns production runs. The systems were kept at 300 K using

the V-rescaling thermostat (the coupling constant was set to 1.0 ps)[55] and at 1 atm employing the Berendsen semi-isotropic barostat. The barostat coupling was set to 2 ps and pressure was applied only in the direction perpendicular to the interface. The van der Waals and Coulomb interactions were cut-off at 1.0 nm and the long-range Coulomb interactions were accounted for using the Particle Mesh Ewald (PME) Method.[56] For decane we used the previously developed united atom force field for hydrocarbons,[57] which was developed together with the SPC model of water.[58] Test calculations show that very similar results were obtained also with the SPCE water model.[58] The water molecules were kept internally rigid using the SETTLE algorithm.[59]

Results and Discussion

The oil droplet/water interface at neutral pH

Vibrational sum frequency scattering (SFS) is a combination of sum frequency spectroscopy and light scattering. SFS, like second harmonic scattering[60–62] is inherently surface sensitive, which makes it a valuable tool to obtain chemical information on interfaces in suspension.[52,63–66] Fig. 1 (left) shows an illustration of a vibrational SFS experiment: a visible and infrared beam are spatially and temporally overlapped in an emulsion, where a simultaneous Raman and infrared process takes place. Since simultaneous Raman and infrared activity is only possible in absence of local inversion symmetry, sum frequency generation takes place exclusively at the droplet surface, where this symmetry is broken. Due to the small size of the droplet, the sum frequency light is emitted in a broad angular scattering pattern with a maximum intensity around θ=55°. We detect at this scattering angle.

Fig 1 (right panel) shows a vibrational SF spectrum of the interface of neat n-hexadecane oil droplets dispersed in D_2O. The ζ-potential of the droplets in this stable emulsion of pure oil in pure water is -55 mV. This value is in excellent correspondence with earlier experiments[17,32] and is commonly employed as a sign of hydroxide surface adsorption. The SFS spectrum detected at

angle θ can be described by the following equation:

$$I_{SFS}(\omega,\theta) \propto \frac{k_0^4}{r^2} I_{IR} I_{VIS} |\Gamma^{(2)}(\theta,R,\omega)|^2 \tag{1}$$

$$\Gamma^{(2)}(\theta,\omega) = Re[\Gamma^{(2)}] + iIm[\Gamma^{(2)}] \tag{2}$$

$$\propto N_s G[F_1(\theta,R);F_2(\theta,R);\boldsymbol{\chi}^{(2)}(\omega)]$$

The scattered intensity depends on the distance between the particle and the detector (r), the scattered wave vector (k_0), the intensity of the IR (I_{IR}) and VIS (I_{VIS}) beams, and on the effective droplet susceptibility $\mathbf{\Gamma}^{(2)}$. The magnitude of $\mathbf{\Gamma}^{(2)}$ is determined by the radius of the droplets (R), the scattering angle (θ), and the surface density of vibrational groups (N_s). The angular direction in which it peaks depends on the scattering form factor functions F_1 and F_2, which are given in e.g. Ref.[67] $\mathbf{\Gamma}^{(2)}$ depends also on the surface susceptibility ($\boldsymbol{\chi}^{(2)}(\omega)$) elements. $\boldsymbol{\chi}^{(2)}(\omega)$ is the orientational averaged product of the IR and Raman tensor components of each vibrational transition that lies within the bandwidth of the IR laser pulse. $\mathbf{\Gamma}^{(2)}$, just like $\boldsymbol{\chi}^{(2)}$, can be expressed as a complex number $Re[\mathbf{\Gamma}^{(2)}]$+i$Im[\mathbf{\Gamma}^{(2)}]$, whereby the relative sign of the real and imaginary part gives information about the relative orientation of the molecular groups present at the droplet interface.[50,68,69]

Since the Fourier transform of our spectrum decays in time, it is possible to use the Maximum Entropy Method (MEM)[70–73] to decompose the spectrum into the imaginary and real parts. MEM analysis is commonly applied in astronomy, economy and other branches of spectroscopy[74–76] and is used to find a solution for the real and imaginary components of a complex power spectrum.[77] Applying MEM analysis to our spectral data, we retrieve the imaginary and real part of $\mathbf{\Gamma}^{(2)}$. The result is plotted in Fig. 1. This reconstruction contains information about the orientation of the water molecules at the interface (in complete analogy with heterodyne detection[50,68]). Since $-Re[\mathbf{\Gamma}^{(2)}]$-i$Im[\mathbf{\Gamma}^{(2)}]$ is also a solution to our mathematical algorithm, we need to make a comparison to oil droplets with a known charge. The average orientation of water on the neat oil/water interface can then be found by comparing the above result to an oil/water interface that is deliberately charged with surfactant. In the next section we will describe the surface structure of

positively and negatively charged oil droplets in water, where we will present both the surfactant, the oil and the water signature by means of selective deuteration. If the water on the neat interface in Fig. 1 has a certain preferred orientation it will match with either the positively charged surface or the negatively charged surface.

Deliberately charged oil droplet/water interfaces

Fig. 2 shows the complex vibrational SF spectra for a number of oil in water emulsions prepared with positively and negatively charged surfactant. The top spectra represent emulsions prepared with positively charged surfactant (CTAB, hexadecyltrimethylammonium bromide), and the bottom spectra represent emulsions prepared with negatively charged surfactant (SDS, sodium dodecylsulfate). The ζ-potentials are ζ = +84 mV, and ζ = -120 mV, respectively. The spectra report the vibrational signature of oil and D_2O (using deuterated surfactant, so that the surfactant resonances are moved out of the spectral window by selective deuteration).

The change in water orientation that accompanies a reversal of charge appears in these spectra as a change in sign of the real part of $\mathbf{\Gamma}^{(2)}$ (as in Ref.[50]). If we compare the positively charged (top) with the negatively charged (bottom) interfaces, we see that indeed the real part has changed sign. The imaginary part reflects the vibrational resonances of the oil alkyl chains at the interface. In the following, we deduce the orientation of the water from the interference of high frequency water bands with the C-H oil modes. Therefore, the relative sign of both Re[$\mathbf{\Gamma}^{(2)}$] and Im[$\mathbf{\Gamma}^{(2)}$] is needed. The imaginary part alone does not suffice, unless the complete resonance is measured and the line shape is purely Lorenztian.[73]

Comparing now the oil/water spectrum of Fig. 1 with the charged oil/water spectra of Fig. 2 we see that the real part of the spectrum of Fig. 1 clearly resembles the spectrum of a negatively charged oil/water surface. Water at the oil droplet/water interface of an emulsion prepared with pure, pH neutral D_2O therefore has an average orientation that is indistinguishable from a negatively charged interface. Whether it requires the surface presence of OH^- ions can be checked by pH dependent SF scattering experiments.

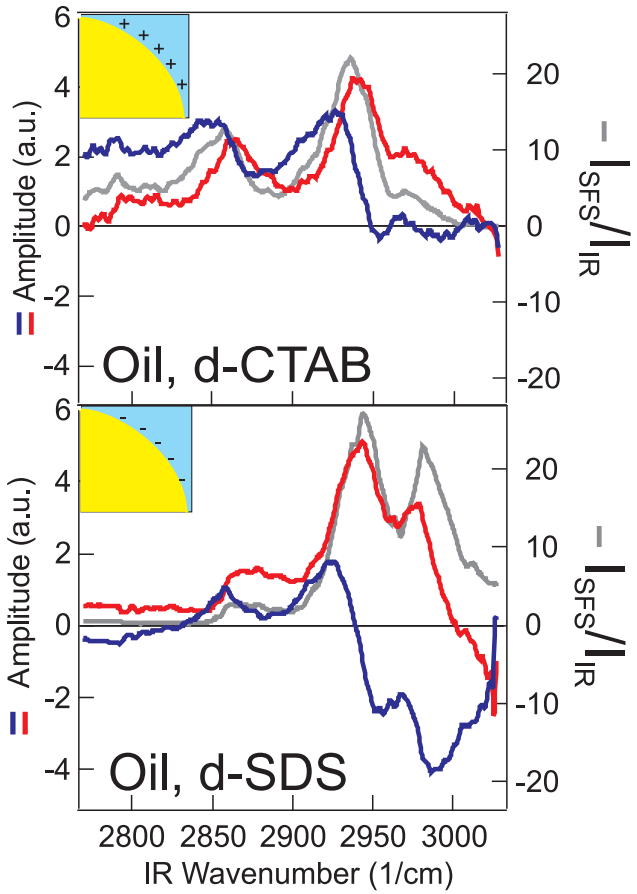

Figure 2: Vibrational SF spectra and the decomposed real and imaginary part of $\Gamma^{(2)}$ (recorded in *ppp*-polarization combination) from 1 vol% n-hexadecane in D_2O emulsion. The droplets have a radius of 100 nm and are prepared with either positively or negatively charged surfactant at critical micelle concentrations. The SF spectrum (grey), the imaginary (red) and real (blue) part of the SF response for a positively charged interface (top: prepared with d-CTAB, and $C_{16}H_{34}$ oil) and a negatively charged interface (bottom: prepared with d-SDS, and $C_{16}H_{34}$ oil). Here the surfactant alkyl chains are deuterated so that the signal reflects the vibrational signature of the $C_{16}H_{34}$ oil and the water. The changing charge results in a change of the phase difference between the real and imaginary part of the signal.

Test of potential surface affinity of OH^- ions

SFG experiments in reflection mode on interfaces of water with a hydrophobic octadecyltrichlorosilane [OTS, $CH_3(CH_2)_{17}SiCl_3$]-covered quartz substrate showed that changing the pH of the bulk water solution changed the spectral appearance of the entire spectral region of water (i.e. 3000 - 3800 cm^{-1}).[38] The interference pattern of surface C-H and O-H stretch modes also changes significantly when the bulk pH is varied from 7 to 11.[36] Ref.[36] shows that the relative phase of Re[$\chi^{(2)}$] and Im[$\chi^{(2)}$] changes significantly when the bulk pH is increased from 7 to 11. The SFG spectra published in Ref.[38] reveal that the amplitude of the water bands that are close in frequency to the CH bands strongly change as a function of pH. For the D_2O/hexadecane water interface, we can expect a similar effect, in the spectral region of 2200 - 3000 cm^{-1}.

If OH^- has a high affinity for the oil droplet/water interface, we may expect a change in the interference between the C-H and water modes, a change in the relative phase between Re[$\Gamma^{(2)}$] and Im[$\Gamma^{(2)}$], or a change in amplitude. We have prepared several surfactant free emulsions with constant droplet size (see Ref.[52] for more information on the procedure) and varying pH, by adjusting the concentration of NaOD from pH neutral to 12.5, corresponding to bulk OH^- concentrations in the range of 1×10^{-4} mM up to 28 mM. The measured ζ potentials are -81 mV, -91 mV and -98 mV, respectively, and can be converted into projected surface charge densities of -0.008 (-0.13), -0.043 (-0.69), -0.42 (-6.75) e/nm^2 (μC/cm^2) using a numerical solution to the nonlinear Poisson-Boltzmann equation (see e.g. p. 19 in Ref.[78]). These values are in good agreement with work reported on similar emulsions, where charge densities are typically reported in the range -0.014 - -0.3 e/nm^2.[17,19,22,32] As was reported in these studies, we have also observed that the bulk pH decreases after emulsion preparation at a pH above pH neutral. This was interpreted as surface adsorption of OH^-.

Fig. 3 shows SFS spectra and the decomposed imaginary and real part of the spectral response in the alkane C-H stretch region and the high frequency part of the O-D stretch spectral region. It is clear that for all four pH values, the spectra and the real and imaginary part are nearly identical. This shows that the average water orientation in a $\sim$1 nm thick slab of water up to the GDS is

unchanged if we increase the pH. Although OH^- can have an effect on the surface chemistry of oil droplets in water, there does not seem to be any evidence of strong specific adsorption of OH^- ions. SF spectra are sensitive to the average (asymmetric) structure of water near the interface. A change in the local surface distribution of water molecules or the polarization fluctuations induced by an enhanced number of OH^- ions at the surface[31,79] would have been observed as either an amplitude change or a relative phase change between $\mathrm{Re}[\Gamma^{(2)}]$ and $\mathrm{Im}[\Gamma^{(2)}]$.

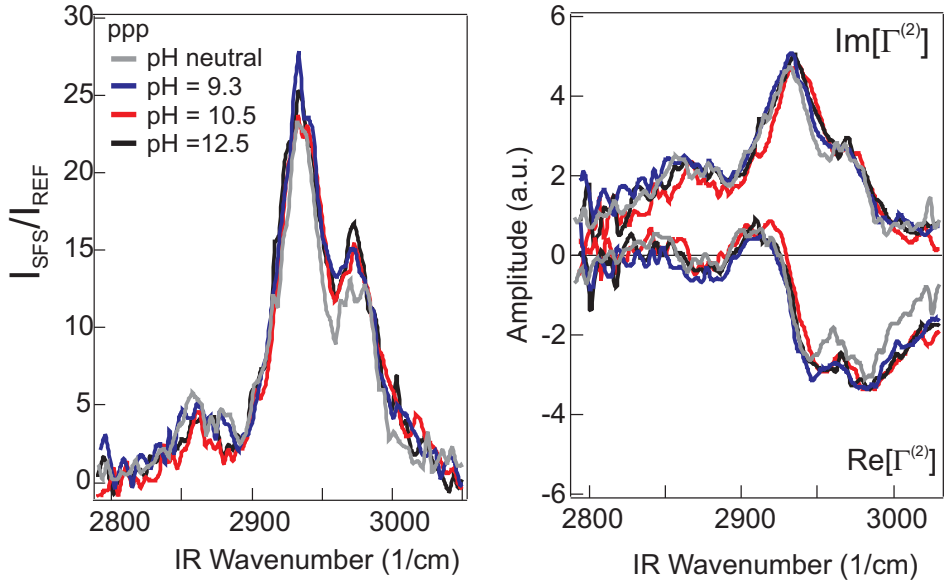

Figure 3: The pH dependence of SF scattering signal. Left: Vibrational SF spectra of the hexadecane oil droplet/water interface at various pH values in ppp polarization. The droplets are in a 1 vol% emulsion and have an average radius of 337 nm. The spectra are not normalized. Right: The imaginary (top) and real (bottom) part of $\Gamma^{(2)}$ as determined using the Maximum Entropy Method.

Alternative explanation of the negative surface charge

Analysis of hydrogen bonding using classical MD

To explain the negative surface charge in the vicinity of the oil/water interface without the need for surface adsorbed hydroxide ions, we consider the consequence of the shift of electron density between different water molecules. Indeed, in the simplest water complex, i.e., the water dimer, there is charge transfer from the hydrogen bond accepting molecule to the hydrogen bond donor. This is due to a shift of electron density from the lone pair on the accepting oxygen to the donating

water molecule.[80]

The magnitude of this charge transfer is not very well established, partly since it is to some extent definition dependent. Values of -0.002 - -0.02 e follow from different population analysis of the water dimer.[81] In larger clusters the degree of charge transfer increases (e.g., -0.038 e in the tetramer[82]). In contrast, in the perfectly tetrahedral arrangement of bulk ice the charge transfer must be zero due to the symmetry between hydrogen bond donating and accepting character of each water molecule. In bulk liquid water, this symmetry is on average pertained, but it can be broken at the anisotropic environment of aqueous interfaces.

To check this possibility, we have first analyzed classical MD simulations of the oil/water interface in terms of the balance between donating and accepting hydrogen bonds in 0.05 nm thick slabs parallel to the interface. Employing a standard hydrogen bond definition (i.e. O-O distance smaller than 0.35 nm and H-O-O angle smaller than 30°[83]) and assigning a value of +1 for each accepting hydrogen bond and a value of -1 for each donating hydrogen bond, we calculated the distribution of hydrogen bonds. The excess of accepting over donating hydrogen bonds along the surface normal are plotted in Fig. 4 (top).

The corresponding cumulative sum represents a measure of the total hydrogen bond asymmetry one encounters if one moves along the surface normal from the oil to the water phase. Approaching the interface from the oil side, the excess is positive up to a depth of 0.25 nm below the GDS and then becomes negative, peaking 0.5 nm below the GDS at -0.07 hydrogen bond per nm^2. Note that this depth of 0.5 nm is close to the estimated position of the slip plane for electrophoretic mobility measurements in water.[84,85] If we use charge transfer values ranging from 0.002 to 0.04 e^- per hydrogen bond, estimated from water cluster studies,[80–82] the hydrogen bond excess of -0.07 nm^{-2} translates to a net negative 'surface' charge of -0.00014 to -0.0028 $1/nm^2$. This is in reasonable agreement with the surface charge densities of -0.008 - -0.42 e/nm^2 that we converted from the ζ-potential values.

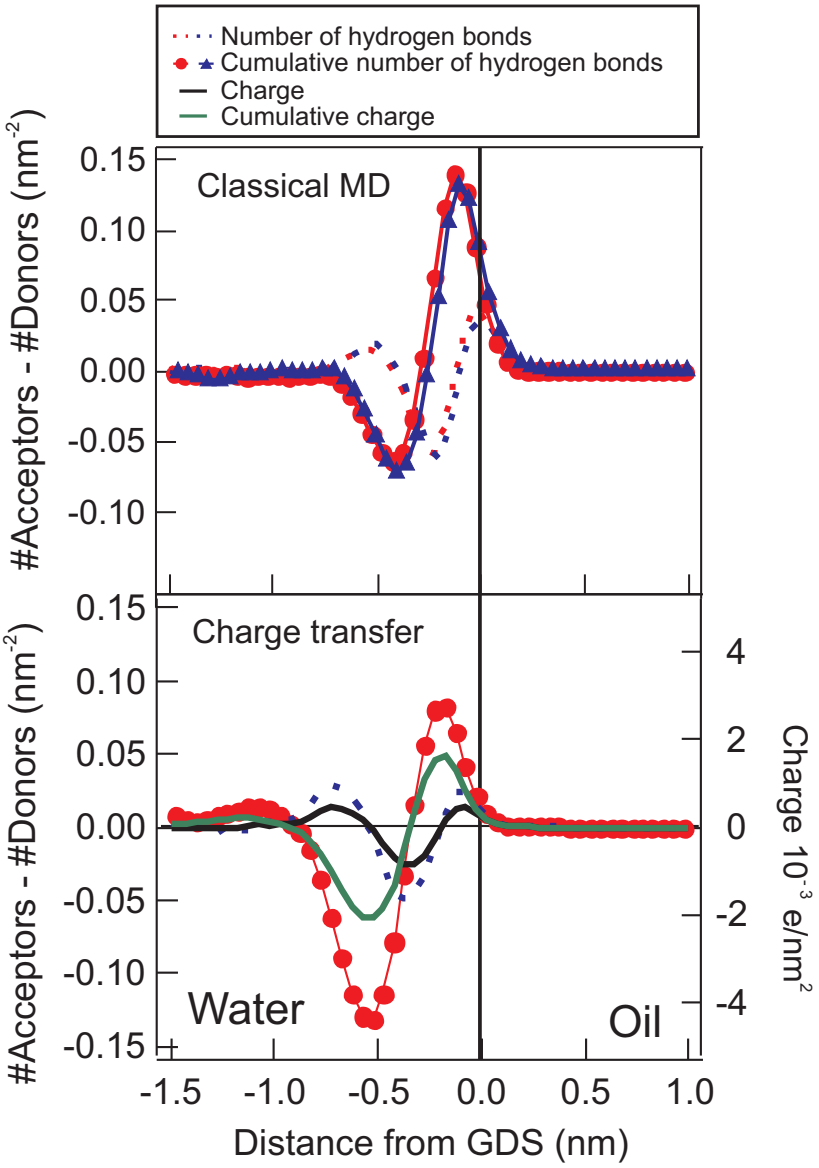

Figure 4: Result of the classical molecular dynamics simulation (top) and the simulation with charge transfer (bottom). Plotted is the balance between accepting and donating hydrogen bonds along the surface normal. The left axis shows the difference in the number of hydrogen bond acceptors and donors. The top plot shows values for a decane surface composed of decane molecules oriented perpendicular (red curves) or parallel (blue curves) with respect to the surface plane. This excess number was obtained for each of the 0.05 nm thick layers by averaging over the whole production run and normalizing per frame and per unit surface area of 1 nm^2. The cumulative profile shows the excess of hydrogen bonds present in the slab located above the point of observation (from oil phase to a given depth). The bottom plot shows the same result using a simulation that allows for charge transfer. The charge is plotted on the right axis. Note that both methods predict a negative charge in the region $\sim$0.3-0.9 nm below the GDS.

MD simulations with charge transfer

To make a more accurate estimate of the above charge transfer hypothesis a water model which includes charge transfer was used to directly examine the effects of charge transfer on the interfacial properties of water. The details of the charge transfer model will be presented elsewhere.[86] Briefly, in this model, charge transfer is added to the polarizable TIP4P-FQ mode[87] by transferring a discrete amount of charge, (δq=-0.02 e), for each hydrogen bond formed, from the hydrogen bond acceptor to the hydrogen bond donor. Here, a hydrogen bond is defined as being made if a distance between a hydrogen and an oxygen is less that 2.3 Å. In order to make the potential continuous, a switching function is added which turns off the amount of charge transferred over a hydrogen-oxygen distance of 2.3 to 2.8 Å. For each amount of charge that is transferred, there is a charge transfer energy, $E_{CT}=\mu_{CT}\delta q+(1/2)\eta_{CT}\delta q^2$,[88] where μ_{CT} is the difference in electronic chemical potential and η_{CT} is the difference in hardness between the two molecules. Using the values from Ref.[88] (μ_{CT}=0.017 a.u/e and η_{CT}=0.491 a.u/e^2) gives a value for E_{CT} equal to -0.15 kcal/mol for δq=-0.02 e. The total charge of a molecule is determined by the difference between that number of hydrogen bonds it forms as a donor (for which it gains -0.02 e of charge per hydrogen bond) and the number it forms as an acceptor (for which it loses -0.02 e of charge). The charge on each atom is then determined by minimizing the energy subject to this charge constraint in a similar manner to the original fluctuating charge model.[87]

The charge transfer model was used to analyze 10,000 configurations from the classical oil/water simulation without charge transfer. The resulting interfacial charge and hydrogen bond asymmetry is presented in Fig. 4 (bottom). The hydrogen bonding profile and the cumulative sum of the acceptor-donor asymmetry are qualitatively the same as for the above classical MD simulations without charge transfer. Also the charge profile follows the same pattern with a positive region right at the interface, which changes to a negative region upon moving into the aqueous phase with maximum negative charge 0.5 nm below the GDS. In absolute terms the amount of charge transfer, -0.002 e/nm^2, is again in agreement with the above estimates based on hydrogen bonding asymmetry and it agrees with the experimental findings.

It should be noted that the results from the MD simulations were obtained for flat interfaces. However, they should be pertinent also for curved interfaced, provided that the curvature is negligible at the molecular scale. In practice, this means that the present MD results are applicable also to curved interfaces with diameter larger than 10-100 nm,[89] such as those investigated experimentally.

Conclusions

In this study we investigated the molecular origin of the exceptional stability of oil emulsions in water and challenged the earlier explanation in terms of strong interfacial adsorption of hydroxide ions. Vibrational sum frequency scattering experiments show that the orientation of water molecules can be followed on the oil droplet/water interface. The water orientation on a neat oil droplet/water interface is practically the same as the water orientation on a negatively charged interface. pH dependent experiments show, however, that there is no sign of selective adsorption of hydroxide ions. Molecular dynamics simulations without and with a term accounting for charge transfer point to a different explanation of the negative interfacial charge, namely, charge transfer between water molecules. Due to a lack of balance between the number of donating and accepting hydrogen bonds of water molecules in the interfacial layer, these water molecules become partially charged. This effect peaks about 0.5 nm below the Gibbs dividing surface and the net negative charge there is estimated to be between -0.00014 to -0.0028 e nm^{-2}. This number has the same sign and is in good agreement with the ζ-potential measurements of the emulsion droplets in this study, being slightly smaller than values estimated from electrophoretic measurements[90] The position of the peak of the negative charge roughly coincides with estimates for the slip plane in electrophoresis of similar systems in aqueous solutions.

Acknowledgments

We thank Dor Ben-Amotz and Daan Frenkel for fruitful discussions. The work done in Stuttgart is part of the research program of the Max Planck Society, while that in Prague was supported via Project Z40550506. Additional funding was received from the German Science Foundation (DFG) under contract number 560398 and the European Research Council (ERC) under contract number 240556. PJ acknowledges support from the Academy of Sciences (Praemium Academie) and the Czech Ministry of Education (Grant LC512). SWR acknowledges support from the National Science Foundation (NSF) under grant number CHE-0611679.

References

(1) Verwey, E. J. W.; Overbeek, J. T. G. *Theory of the stability of lyophobic colloids*; Dover Publications, 1948.

(2) Hunter, R. J. *Foundations of Colloid Science*; 2002.

(3) Zangi, R.; Engberts, J. B. F. N. *J. Am. Chem. Soc.* **2005**, *127*, 2272–2276.

(4) Kudin, K. N.; Car, R. *J. Am. Chem. Soc.* **2008**, *130*, 3915–3919.

(5) Vacha, R.; Horinek, D.; Berkowitz, M. L.; Jungwirth, P. *Phys. Chem. Chem. Phys.* **2008**, *10*, 4975–4980.

(6) Weissenborn, P. K.; Pugh, R. J. *J. of Coll. Int. Sci.* **1996**, *184*, 550–563.

(7) Petersen, M. K.; Iyengar, S. S.; Day, T. J. F.; Voth, G. A. *J. Phys. Chem. B* **2004**, *108*, 14804–14806.

(8) Iyengar, S. S.; Day, T. J. F.; Voth, G. A. *Int. J. Mass Spec.* **2005**, *241*, 197–204.

(9) Petersen, P. B.; Saykally, R. J. *J. Phys. Chem. B* **2005**, *109*, 7976–7980.

(10) Petersen, P. B.; Saykally, R. J. *Chem. Phys. Lett.* **2008**, *458*, 255–261.

(11) Tarbuck, T. L.; Ota, S. T.; Richmond, G. L. *J. Am. Chem. Soc.* **2006**, *128*, 14519–14527.

(12) Winter, B.; Faubel, M.; Vacha, R.; Jungwirth, P. *Chem. Phys. Lett.* **2009**, *474*, 241–247.

(13) Buch, V.; Milet, A.; Vacha, R.; Jungwirth, P.; Devlin, J. P. *Proc. Nat. Am. Sci.* **2007**, *104*, 7342–7347.

(14) Wick, C. D.; Kuo, I. F. W.; Mundy, C. J.; Dang, L. X. *J. Chem. Theory Comput.* **2007**, *3*, 2002–2010.

(15) Mundy, C. J.; Kuo, I. F. W.; Tuckerman, M. E.; Lee, H. S.; Tobias, D. J. *Chem. Phys. Lett.* **2009**, *481*, 2–8.

(16) Graciaa, A.; Morel, G.; Saulner, P.; Lachaise, J.; Schechter, R. *J. Coll. Int. Sci.* **1995**, *172*, 131–136.

(17) Marinova, K. G.; Alargova, R. G.; Denkov, N. D.; Velev, O. D.; Petsev, D. N.; Ivanov, I. B.; Borwankar, R. P. *Langmuir* **1996**, *12*, 2045–2051.

(18) Stachurski, J.; Michalek, M. *J. Coll. Interface Sci.* **1996**, *184*, 433–436.

(19) Stubenrauch, C.; von Klitzing, R. *J. Phys. Condens. Matter.* **2003**, *15*, R1197.

(20) Takahashi, M. *J. Phys Chem. B* **2005**, *109*, 21858–21864.

(21) Zilch, L. W.; Maze, J. T.; Smith, J. W.; Ewing, G. E.; Jarrold, M. F. *J. Phys. Chem. A* **2008**, *112*, 13352–13363.

(22) Beattie, J. K.; Djerdjev, A. M. *Angew. Chem. Int. Ed.* **2004**, *43*, 3568 – 3571.

(23) Beattie, J. K. *Phys. Chem. Chem. Phys* **2007**, *10*, 330–331.

(24) Leunissen, M. E.; van Blaaderen, A.; Hollingsworth, A. D.; Sullivan, M. T.; Chaikin, P. M. *Proc. Nat. Acad. Sci.* **2007**, *104*, 2585–2590.

(25) Tandon, V.; Bhagavatula, S. K.; Nelson, W. C.; Kirby, B. J. *Electrophoresis* **2008**, *29*, 1092–1101.

(26) Beattie, J. K.; Djerdjev, A. N.; Warr, G. G. *Faraday Discussions* **2009**, *141*, 31–39.

(27) Zimmermann, R.; Freudenberg, U.; Schweiss, R.; Kuttner, D.; Werner, C. *Curr. Opin. Coll. Int. Sci.* **2010**, *15*, 196–202.

(28) Bonthuis, D. J.; Horinek, D.; Bocquet, L.; Netz, R. R. *Langmuir* **2010**, *26*, 12614–12625.

(29) Hunter, R. J. In *Zeta potential in colloid science*; Ottewill, R. H., Rowell, R. L., Eds.; Academic Press, 1981.

(30) Delgado, A. V.; González-Caballero, F.; Hunter, R. J.; Koopal, L. K.; Lyklema, J. *Pure Appl. Chem.* **2005**, *77*, 1753Ű1805.

(31) Gray-Weale,; Beattie, J. *Phys. Chem. Chem. Phys.* **2009**, *11*, 10994–11005.

(32) Creux, P.; Lachaise, J.; Graciaa, A.; Beattie, J. K.; Djerdjev, A. M. *J. Phys. Chem. B* **2009**, *113*, 14146–14150.

(33) Sakai, T. *Curr. Op. Coll. Int. Sci.* **2008**, *13*, 228–235.

(34) Conboy, J. C.; Daschbach, J. L.; Richmond, G. L. *Appl. Phys. A* **1994**, *59*, 623–629.

(35) Scatena, L. F.; Brown, M. G.; Richmond, G. L. *Science* **2001**, *292*, 908–912.

(36) Ye, S.; Nihonyanagi, S.; Uosaki, K. *Phys. Chem. Chem. Phys.* **2001**, *3*, 3463–3469.

(37) Brown, M.; Walker, D.; Raymond, E.; Richmond, G. *J. Phys. Chem. B* **2003**, *107*, 237–244.

(38) Tian, C. S.; Shen, Y. R. *Proc. Nat. Ac. Sci.* **2009**, *106*, 15148–15153.

(39) Goebel, K., A. K. Lunkenheimer *Langmuir* **1997**, *13*, 369–372.

(40) Shultz, M. J.; Schnitzer, C.; Simonelli, D.; Baldelli, S. *Int. Rev. Phys. Chem.* **2000**, *19*, 123–153.

(41) Richmond, G. L. *Chem. Rev.* **2002**, *102*, 2693–2724.

(42) Shen, Y. R.; Ostroverkhov, V. *Chem. Rev.* **2006**, *106*, 1140–1154.

(43) Ji, N.; Ostroverkhov, V.; Tian, C. S.; Shen, Y. R. *Phys. Rev. Lett.* **2008**, *100*.

(44) Sovago, M.; Campen, R. K.; Bakker, H. J.; Bonn, M. *Chem. Phys. Lett.* **2009**, *470*, 7–12.

(45) Tian, C. S.; Shen, Y. R. *Chem. Phys. Lett.* **2009**, *470*, 1–6.

(46) Walker, D. S.; Moore, F. G.; Richmond, G. L. *J. Phys. Chem. C* **2007**, *111*, 6103–6112.

(47) Knecht, V.; Risselada, H. J.; Mark, A. E.; Marrink, S. J. *J. Coll. Int. Sci.* **2008**, *318*, 477–486.

(48) Knecht, V.; Zachary A. Levine, Z. A.; P. Thomas Vernier, P. T. *J. Coll. Int. Sci.* **2010**, *352*, 223–231.

(49) de Aguiar, H. B.; Samson, J.-S.; Roke, S. *submitted*

(50) Nihonyanagi, S.; Yamaguchi, S.; Tahara, T. *J. Chem. Phys.* **2009**, *130*, 204704.

(51) Sugiharto, A. B.; Johnson, C. M.; de Aguiar, H. B.; Aloatti, L.; Roke, S. *Appl. Phys. B.* **2008**, *91*, 315–318.

(52) de Aguiar, H. B.; de Beer, A. G. F.; Strader, M. L.; Roke, S. *J. Am. Chem. Soc.* **2010**, *132*, 2122–2123.

(53) Lunkenheimer, K.; Pergande, H.-J.; Krueger, H. *Rev. Sci. Instrum.* **1987**, *58*, 2313–2318.

(54) Hess, B.; Kutzner, C.; van der Spoel, D.; Lindahl, E. *J. Chem. Theory Comp.* **2008**, *4*, 435–447.

(55) Bussi, G.; Donadio, D.; Parrinello, M. *J. Chem. Phys.* **2007**, *126*.

(56) Darden, T.; York, D.; Pedersen, L. *J. Chem. Phys.* **1993**, *98*, 10089–10092.

(57) W. F. van Gunsteren and H. J. C. Berendsen. Gromos-87 manual. Biomos BV,. Nijenborgh 4, 9747 AG Groningen, The Netherlands, 1987. 1987.

(58) Berendsen, H. J. C.; Grigera, J. R.; Straatsma, T. P. *J. Phys. Chem.* **1987**, *91*, 6269–6271.

(59) Miyamoto, S.; Kollman, P. A. *J. Comp. Chem.* **1992**, *13*, 952–962.

(60) Wang, H.; Yan, E. C. Y.; Borguet, E.; Eisenthal, K. B. *Chem. Phys. Lett.* **1996**, *259*, 15–20.

(61) Yan, E. C. Y.; Liu, Y.; Eisenthal, K. B. *J. Phys. Chem. B* **1998**, *102*, 6331–6336.

(62) Eisenthal, K. B. *Chem. Rev.* **2006**, *106*, 1462–1477.

(63) Roke, S.; Roeterdink, W. G.; Wijnhoven, J. E. G. J.; Petukhov, A. V.; Kleyn, A. W.; Bonn, M. *Phys. Rev. Lett.* **2003**, *91*, 258302.

(64) Roke, S.; Buitenhuis, J.; van Miltenburg, J. C.; Bonn, M.; van Blaaderen, A. *J. Phys. Cond. Matter* **2005**, *17*, S3469–S3479.

(65) de Beer, A. G. F.; Roke, S. *Phys. Rev. B* **2007**, *75*, 245438.

(66) Roke, S. *Chem. Phys. Chem.* **2009**, *10*, 1380–1388.

(67) de Beer, A. G. F.; Roke, S. *J. Chem. Phys.* **2010**, *132*, 234702.

(68) Ostroverkhov, V.; Waychunas, G. A.; Shen, Y. R. *Phys. Rev. Lett.* **2005**, *94*.

(69) Tian, C. S.; Ji, N.; Waychunas, G.; Shen, Y. R. *J. am. Chem. Soc.* **2008**, *130*, 13033–13039.

(70) Burg, J. P. Maximum Entropy Spectral Analysis. Ph.D. thesis, Stanford University, 1975.

(71) Haykin, S.; Kesler, S. In *Prediction-Error Filtering and Maximum-Entropy Spectral Estimation*; Haykin, S., Ed.; Springer Verlag, 1983; Chapter 2, pp 9–70.

(72) Sovago, M.; Vartiainen, E.; Bonn, M. *J. Phys. Chem. C* **2009**, *113*, 6100–6106.

(73) de Beer, A. G. F.; Campen, R. K.; Roke, S. *Phys. Rev. B* **2010**, *82*, 1–6.

(74) Sibisi, S.; Skilling, J.; Brereton, R. G.; Laue, E. D.; Staunton, J. *Nature* **1984**, *311*, 446–447.

(75) Narayan, *Ann. Rev. of Astronomy and Astrophysics* **1986**, *24*, 127.

(76) Kitaura, R.; Kitagawa, S.; Kubota, Y.; Kobayashi, T. C.; Kindo, K.; Mita, Y.; Matsuo, A.; Kobayashi, M.; Chang, H. C.; Ozawa, T. C.; Suzuki, M.; Sakata, M.; Takata, M. *Science* **2002**, *298*, 2358–2361.

(77) Haykin, S.; Kesler, S. In *Prediction-Error Filtering and Maximum-Entropy Spectral Estimation*; Haykin, S., Ed.; Springer Verlag, 1983; Chapter 2, pp 9 – 70.

(78) Oshima, H. *Theory of Colloid and Interfacial phenomena*; Academic Press, 2006.

(79) Chen, B.; Park, J.; Ivanov, I.; Tabacchi, G.; Klein, M.; Parrinello, M. *J. Am. Chem. Soc.* **2002**, *124*, 8534–8535.

(80) Galvez, O.; Gomez, P. C.; Pacios, L. F. *J. Chem. Phys.* **2001**, *115*, 11166.

(81) Rustam, Z. K.; Bell, A. T.; Head-Gordon, M. *Chem. Eur. J.* **2009**, *15*, 851–855.

(82) Glendening, E. D. *J. Phys. Chem. A* **2005**, *109*, 11936–11940.

(83) Luzar, D., A. amd Chandler *Nature* **1996**, *379*, 55–57.

(84) Lyklema, J. *Colloids Surf., A* **1994**, *92*, 41–49.

(85) Mattke, T.; Kecke, H. J. *J. Coll. Int. Sci.* **1998**, *208*, 555–561.

(86) Lee, A. J.; Rick, S. W. *J. Chem. Phys. in press* **2011**,

(87) Rick, S.; Stuart, S.; Berne, B. *J. Chem. Phys.* **1994**, *101*, 6141–6156.

(88) Korchowiec, J.; Uchimaru, T. *J. Chem. Phys.* **2000**, *112*, 1623–1633.

(89) Stuart, S. J.; Berne, B. J. J. *J. Phys. Chem. A* **1999**, *103*, 10300 – 10307.

(90) Karraker, K. A.; Radke, C. J. *Adv. Coll. Int. Sci.* **2002**, *96*, 231–264.